1994

Use of Underpotential Deposition of Zinc to Mitigate Hydrogen Absorption into Monel K500

G. Zheng
University of South Carolina - Columbia

Branko N. Popov
University of South Carolina - Columbia, popov@engr.sc.edu

Ralph E. White
University of South Carolina - Columbia, white@cec.sc.edu

Publication Info

Journal of the Electrochemical Society, 1994, pages 1220-1224.

17. J. H. von Barner, E. Christensen, N. J. Bjerrum, and B. Gilbert, *Inorg. Chem.*, **30**, 561 (1991).
18. M. Sakawa and T. Kuroda, *Denki Kagaku*, **36**, 146 (1968); (*C.A.*, **69**, 24075d).
19. G. W. Horsby, *J. Iron Steel Inst.*, p. 43 (1956).
20. H. W. Jenkins, G. Mamantov, and D. L. Manning, *J. Electroanal.Chem.*, **19**, 385 (1968).
21. F. Matthiesen, E. Christensen, J. H. von Barner, and N. J. Bjerrum, To be published.

Use of Underpotential Deposition of Zinc to Mitigate Hydrogen Absorption into Monel K500

G. Zheng,* B. N. Popov, and R. E. White****

Department of Chemical Engineering, University of South Carolina, Columbia, South Carolina 29208

ABSTRACT

Polarization experiments and a potentiostatic pulse technique have been used to show that a monolayer coverage of zinc effectively inhibits the absorption of hydrogen into Monel K500. By depositing a monolayer of zinc on Monel K500, the hydrogen evolution reaction and hydrogen ingress flux rate were reduced by 60%.

The practical use of high strength alloys is limited by cracking hazards created by the penetration and accumulation of hydrogen in the bulk of the alloy.[1,2] The sources of hydrogen causing embrittlement have been encountered in electroplating, in pickling operations, in the processes of corrosion or rusting during storage and transportation, and in the process of cathodic protections. When weakening alloys, the hydrogen will tend to accumulate in areas of high stress, and it may reach a critical hydrogen concentration. At this point microcracking will occur and may lead to a catastrophic fracture that damages the part.[3-5] Also, in the presence of absorbed hydrogen, changes occur in both the lattice structure and the chemical composition of the alloy.[6]

Various methods have been proposed to decrease hydrogen embrittlement.[7-10] Among these methods are post-heat-treatment, alloying addition, laser surface modification, and shot peening. However, when using these methods, it is difficult to reduce hydrogenation of the alloy to a level which eliminates the cracking hazards.

Drazic and Vorkapic[11] established that the presence of metal ions (Cd^{+2}, and Zn^{+2}) that are more electronegative than the cathodic potential for the hydrogen evolution reaction on iron in a 0.25*M* H_2SO_4 solution inhibits the hydrogen evolution reaction and corrosion of iron. This effect has been explained as the underpotential deposition (UPD) of the adatoms of these metals on iron. By comparing cyclic voltammetry results with data derived from the Devanathan-Stachurski method (under identical conditions), it was shown that the underpotential adsorption of zinc, bismuth, and lead onto AISI 4340 steel and Inconel 718 reduced the amount of both atomic hydrogen adsorbed and the degree of hydrogen ingress in the substrate.[12-16]

The objective of this work was to estimate the effectiveness of the UPD of zinc on the reduction of the hydrogen evolution rate and on the degree of hydrogen ingress into Monel K500. A monolayer of zinc was expected to reduce the surface coverage of adsorbed hydrogen and change the kinetic parameters of the hydrogen discharge reaction, thereby inhibiting the corrosion rate and reducing the absorption of hydrogen into Monel K500.

Experimental

Tafel and linear sweep voltammetry were used to investigate the possibility of the underpotential deposition of zinc on Monel K500, and to determine the diagnostic criteria for the identification of the mechanism of hydrogen discharge in the presence and absence of underpotential deposited zinc. These techniques were also used to determine the experimental UPD conditions. A potentiostatic pulse technique, developed by Pound *et al.*,[17,18] was used to estimate the rate of hydrogen ingress into the alloy.

The electrochemical cell employed for the Tafel method, the linear sweep voltammetry studies, and the potentiostatic pulse technique was a conventional three-compartment design with contact between the working electrode compartment and the reference electrode via a Luggin probe. The reference electrode was a saturated calomel electrode (SCE), and the auxiliary electrode was a platinum gauze with a high surface area. The experiments were conducted using the Model 342C SoftCorr System with the EG&G Princeton Applied Research potentiostat/galvanstat Model 273 at room temperature (23 ± 1°C). ACS Reagent chemicals were used to prepare a 1*M* Na_2SO_4, 0.4*M* NaCl, and 1*M* H_3BO_3 supporting electrolyte. Several hours before the experiments were conducted, the electrolyte was degassed by passing prepurified nitrogen through the solution. The Monel K500 electrode (geometric area of 0.5 cm^2) was inserted into a Teflon holder so that only the flat surface was exposed. The composition of the alloy in weight percent (w/o) is: Al 2.92, C 0.16, Cu 29.99, Fe 0.64, Mn 0.72, Ni 64.96, S 0.001, Si 0.15, and Ti 0.46. Prior to each run, the electrode surface was mechanically polished with 600 grade SiC paper followed by 0.05 μm aluminum powder to mirror finish, cleaned in an ultrasonic cleaning bath, and thoroughly rinsed with deionized water.

By using the potentiostatic pulse technique, the rate of hydrogen absorption into the Monel K500 electrode and the trapping constant in the presence and absence of zinc was estimated from experimental data. The test electrode was charged at a constant cathodic potential of $E_c = -1.0$ V *vs.* SCE, which gives a monolayer deposition of zinc, for a time between 1 to 30 s. Then the potential was increased to a more positive value E_A (10 mV more negative than the open-circuit potential E_{oc}). The cathodic/anodic current and total charge accumulation during the cathodic charge/anodic discharge process was measured simultaneously by the potentiostat/galvanostat and a recorder. The experimental results were checked by repeating the experiment for the charging time of 1 s to insure that neither hydrogen saturation nor internal damage occurred during the cathodic charge process. The details of this technique are explained by Pound.[17,18]

Results and Discussion

Cyclic voltammetry.—Figure 1 shows the linear sweep voltammetric curves which were obtained in the absence and presence of zinc ions on Monel K500 electrodes by using an electrolyte containing 1*M* Na_2SO_4, 0.4*M* NaCl, and 1*M* H_3BO_3 (pH 4) at sweep rate of 100 mV as shown in Fig. 1. A decrease in hydrogen evolution was observed when the experiments were carried out in the presence of 5×10^{-3}

* Electrochemical Society Student Member.
** Electrochemical Society Active Member.

Zn^{+2} rather than in the absence of zinc ions. When starting the cathodic sweep from −0.50 V *vs.* SCE, two cathodic peaks were observed in the presence of $5 \times 10^{-3}M$ of zinc ions. The first peak occurred at a potential of about −0.88 V *vs.* SCE, which is more positive than the reversible Nernst potential ($E_{rev} = -1.07$). Here, the first peak corresponded to the underpotential deposition of zinc on the Monel. The second peak occurred at a potential of −1.15 V *vs.* SCE, which is more negative than the Nernst potential. This peak represents the bulk deposition of zinc on the electrode. The two anodic peaks observed are corresponding stripping peaks. Since the underpotential peaks are not clearly visible in Fig. 1 because of the large scale of current density, the enlarged peaks for the concentration of $5 \times 10^{-3}M$ of zinc are shown in Fig. 2. The degree of coverage by zinc in the underpotential deposition can be estimated by integrating the corresponding peak's area, which gives a charge of about 400 $\mu C/cm^2$. According to Frumkin,[19] the maximum coverage of a monolayer of zinc requires a charge of 450 $\mu C/cm^2$, when the surface roughness factor is 1, the degree of coverage by UPD zinc is about 0.9.

Tafel method.—Cathodic polarization curves were obtained for the evolution of hydrogen on a zinc-free Monel K500 electrode surface in an electrolyte containing $1M$ Na_2SO_4, $0.4M$ NaCl, and $1M$ H_3BO_3, and on a Monel K500 surface predeposited with zinc from the same electrolyte in which $5 \times 10^{-3}M$ of Zn^{+2} was added. In order to deposit zinc, the electrode (with an area of 0.5 cm^2) was held at different cathodic potentials for 5 min each to ensure that zinc deposited on the surface. Then, the experiment was started. The bulk deposition of zinc occurred on the surface when

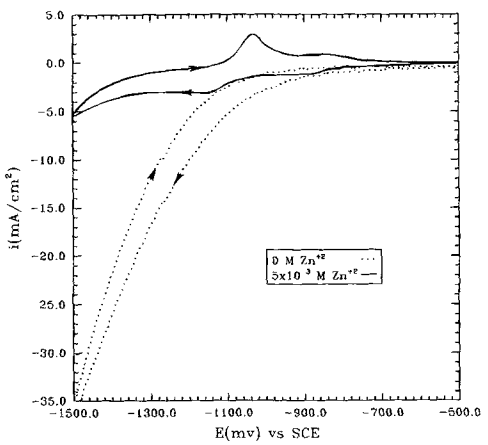

Fig. 1. Cyclic voltammetry curves obtained on Monel K500, using an electrolyte containing $1M$ N_2SO_4, $0.4M$ NaCl, and $1M$ H_3BO_3 in the absence and presence of Zn^{+2}, and sweep rate = 100 mV/s.

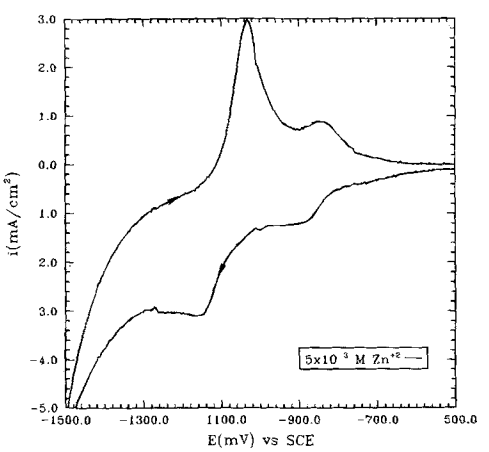

Fig. 2. The enlarged cyclic voltammetry curve presented in Fig. 1 for the concentration of $5 \times 10^{-3}M$ Zn^{+2}.

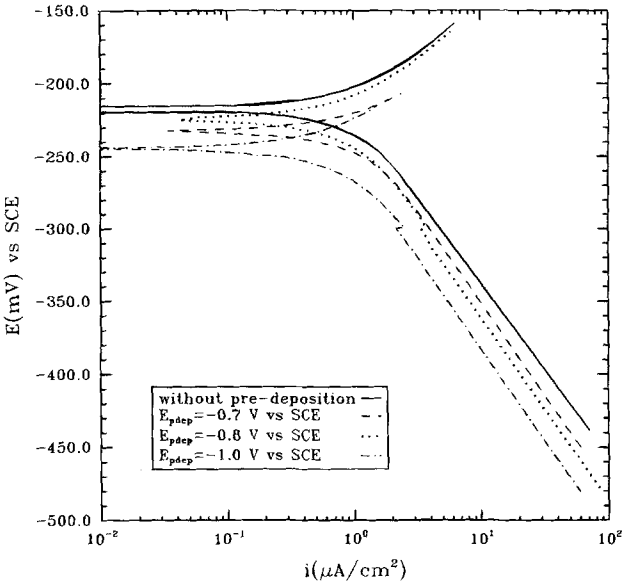

Fig. 3. Tafel curves obtained on Monel K500 with and without the predeposition of zinc on the substrate, the predeposition time 5 min, sweep rate = 1 mV/s.

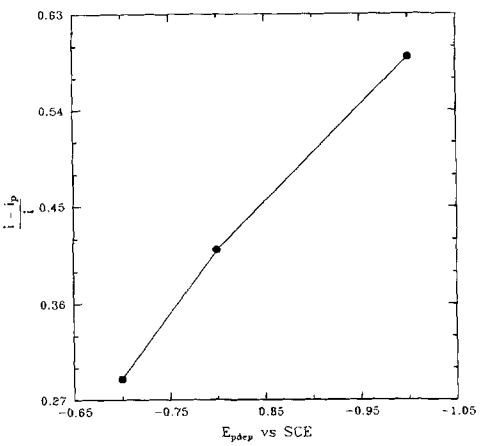

Fig. 4. Dependence of hydrogen evolution current on Monel K500 electrode computed at −400 mV (SCE) from Fig. 3 as a function of the applied predeposition potential.

the applied potential was at −1.10 V *vs.* SCE, which is consistent with the results in the cyclic voltammetry studies. Three predeposition potentials, more positive than −1.10 V *vs.* SCE, (namely, −1.0, −0.80, and −0.700 V *vs.* SCE), were applied to obtain different coverages of zinc on the surface. The cathodic polarization curves obtained for the hydrogen evolution reaction both on the Zn-free Monel K500 and the zinc-covered Monel K500 are shown in Fig. 3. The Tafel slopes are in the range from 118 to 125 mV/decade. According to literature,[1,20] Tafel slope of 118 to 125 mV/decade indicates eight possible hydrogen evolution mechanisms, namely: slow discharge-fast recombination mechanism and coupled discharge-electrochemical mechanism, each with various isotherms (Langmuir isotherm, Temkin isotherm for nonactivated adsorption, and Temkin isotherm for activated adsorption) and the last two are the slow discharge-fast electrochemical desorption mechanism and coupled discharge-recombination mechanism with Langmuir isotherm. The first six possible mechanisms predict that the steady-state hydrogen permeation current is independent of the applied cathodic current density, while the slow discharge-fast electrochemical desorption mechanism predicts that the steady-state hydrogen permeation current is reversely proportional to the square of the cathodic current. These mechanisms cannot be applied to ex-

plain the experimental observations for hydrogen discharge on nickel and its alloys where the steady-state hydrogen permeation current is directly proportional to the square root of the cathodic current.[21,22] The only reasonable explanation of the observed experimental data is the coupled discharge-recombination mechanism which predicts square root relationship between the steady-state hydrogen permeation current and applied cathodic current.[22] As seen in Fig. 3, the presence of zinc monolayer on the surface of Monel K500 inhibited the hydrogen evolution reaction (HER). For example, the hydrogen evolution current density was reduced from 34 $\mu A/cm^2$ (on the zinc-free electrode) to 14 $\mu A/cm^2$ (on the electrode previously deposited with zinc at potential −1.0 V *vs.* SCE). The results obtained from the polarization studies are summarized in Fig. 4 in which the hydrogen evolution current $(i - i_p/i)$ at −400 mV *vs.* SCE in the presence (i_p) and absence (i) of a predeposited monolayer of zinc on the alloy surface is plotted as a function of the predeposited potentials. The HER is reduced by 60% when compared with the corresponding value obtained on a bare Monel K500 surface. Note that no bulk deposition was possible during the experiments because the potential range in the experiments was more noble than the zinc reversible potential (−1.10 V *vs.* SCE).

Potentiostatic pulse technique.—A diffusion/trapping model used to analyze the anodic transients was previously developed[17,18] by solving the modified version of Fick's second law which includes a trapping term $(k_a c)$

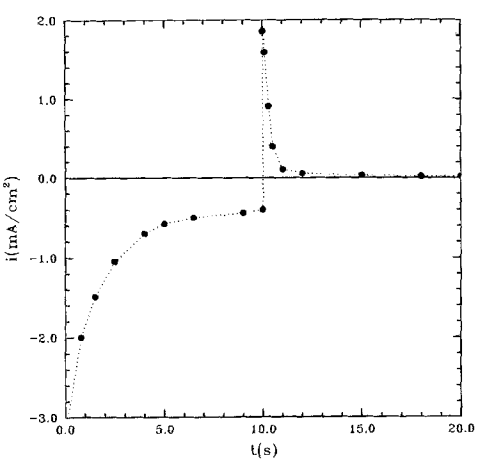

Fig. 5. A typical cathodic and anodic transient for Monel K500 in the electrolyte containing 1*M* Na_3SO_4, 0.4*M* NaCl, and 1*M* H_3BO_3 in the presence of 5 × 10^{-3}*M* of Zn^{+2}, t_c = 10 s, E_c = −1.0 V.

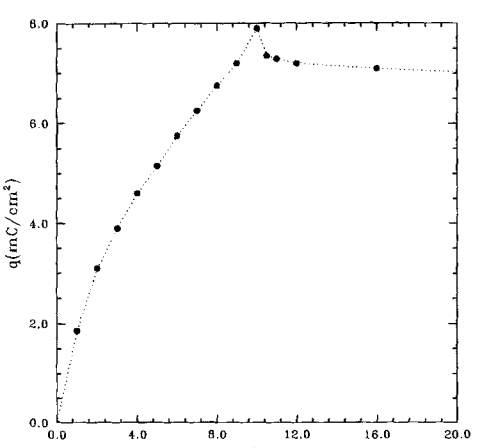

Fig. 6. A typical charge accumulation during the charge and discharge process for Monel K500 in an electrolyte containing 1*M* Na_2SO_4, 0.4*M* NaCl, and 1*M* H_3BO_3 in the presence of 5 × 10^{-3}*M* Zn^{+2}, t_c = 10 s, E_c = −1.0 V.

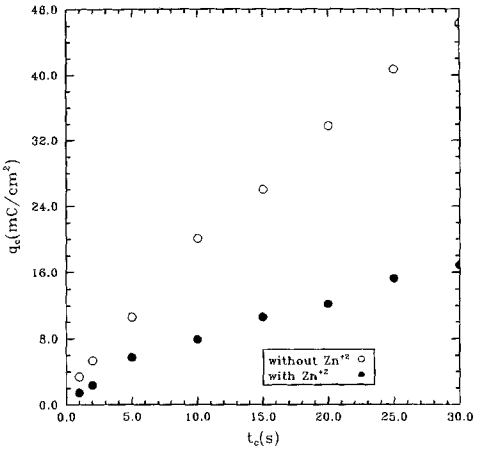

Fig. 7. Dependence of experimental cathodic charge (q_c) on charging time (t_c) for Monel K500 in the absence and presence of 5 × 10^{-3}*M* of zinc ions.

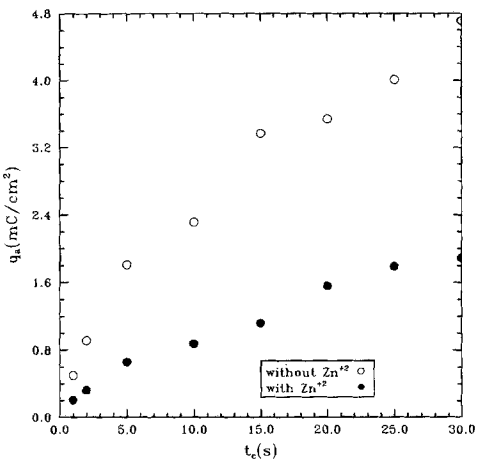

Fig. 8. Dependence of experimental charge passed out (q_a) on charging time (t_c) for Monel K500 in the absence and presence of 5 × 10^{-3}*M* Zn^{+2}.

$$\frac{\partial c}{\partial t} = D_a \frac{\partial^2 c}{\partial^2 x} - k_a c \qquad [1]$$

where c is the hydrogen concentration in the metal in mol/cm^3, D_a is the apparent diffusion coefficient, (cm^2/s), and k_a is the apparent trapping constant in s^{-1}. This equation has been solved analytically in term of two cases, namely, (*i*) pure diffusion control, in which the hydrogen atom absorption rate is determined by the diffusion in the metal, and (*ii*) diffusion control with finite surface kinetics, in which the hydrogen absorption rate is controlled by the flux across the interface. Assuming that the trapping is irreversible, the first-order process and the charging time is short enough so that the trapping sites are not saturated or generated, *i.e.*, the trapping constant (k_a) remains constant during the times of interest.

The experimental data analyzed by a pure diffusion control model indicated that the trapping constant varied with charging time, which contradicts the assumption of the model. Therefore, the pure diffusion control model is not valid for our experimental results. This conclusion is the same as that obtained by Pound for AISI 4340, Monel K500, and other metals and alloys.[23-27] The diffusion control with finite surface kinetics model, therefore, was used to analyze the data. According to this model, the total nondimensional charge passed out during the anodic discharge process is

$$Q'_{(\infty)} = \sqrt{R}\left\{1 - \frac{e^{-R}}{\sqrt{\pi R}} - \left[1 - \frac{1}{2R}\right]\operatorname{erf}\sqrt{R}\right\} \quad [2]$$

The total dimensionless charge passed in is

$$Q_{in} = \sqrt{R} \quad [3]$$

and the trapped charge is given by

$$Q_T = \sqrt{R}\left\{1 - \frac{e^{-R}}{\sqrt{\pi R}} + \left[1 - \frac{1}{2R}\right]\operatorname{erf}\sqrt{R}\right\} \quad [4]$$

where the dimensionless terms are defined by

$$Q = \frac{q}{FJ\sqrt{t_c/k_a}} \quad [5]$$

$$R = k_a t_c \quad [6]$$

q is the charge density in C/cm^2, t_c is the charging time in s, J is the ingress flux in mol cm^{-2} s^{-1}, and F is Faraday's constant. Since the adsorbed charge (q_{ads}) in C/cm^2 is invariably found to be negligible,[17,18] the q_a can be associated with absorbed hydrogen and is approximately equal to the anodic charge $q'_{(\infty)}$ corresponding to $Q'_{(\infty)}$. The apparent trapping constant k_a (measured for irreversible traps in the presence of reversible traps) can be expressed by $k(D_a/D_L)$, where k is the irreversible trapping constant in s^{-1}, D_a is the apparent diffusivity, and D_L is the lattice diffusivity of hydrogen in the metal.

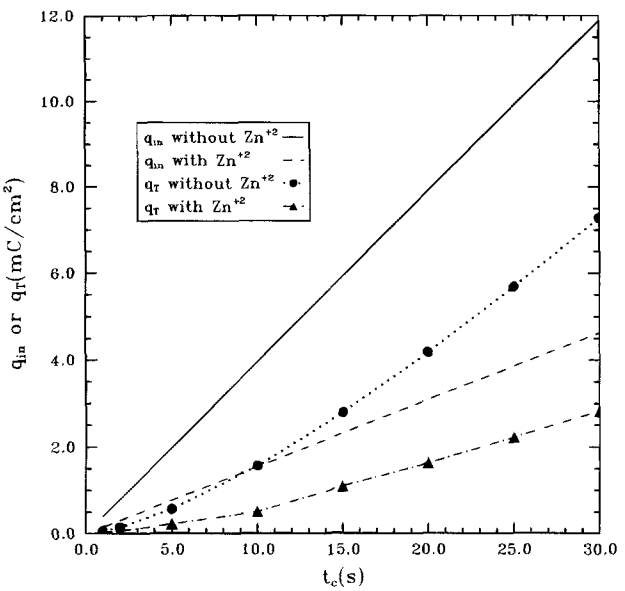

Fig. 9. Dependence of q_{in} and q_T on the charging time in the absence and presence of $5 \times 10^{-3}M$ zinc ions.

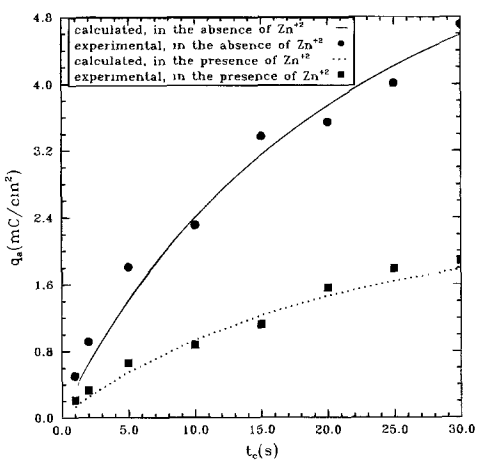

Fig. 10. Comparison of experimental charge data passed out with the calculated values for Monel K500 in the presence and absence of zinc ions.

All experimental cathodic/anodic current transients and charge accumulation show the same shape of curves. Typical cathodic/anodic current transients and charge accumulation are shown in Fig. 5 and 6, respectively. The experimental data of the charge passed out (q_a) and the total cathodic charges (q_c) in the presence and absence of zinc ions were presented in Fig. 7 and 8 as functions of charging time.

The data were analyzed by adjusting the trapping constant (k_a) in Eq. 2 and 5 until the rate of ingress was constant for all of the charging time (t_c). By this method, a k_a value of 0.031 s^{-1} was obtained in the presence and absence of zinc ions; the corresponding two flux values are 1.6×10^{-9} and 4.1×10^{-9} mol/(cm^2 s), respectively. This k_a value (0.031 s^{-1}) is close to Pound's values (0.017 to 0.027 s^{-1}) for as-received Monel K500.[23,24] The value of the ingress flux (J) is one order of magnitude higher than Pound's results (0.15 to 0.21×10^{-9} mol/(cm^2 s). However, the present electrolyte is different from that used by Pound. Pound used an acetate buffer, pH 4.8.

Using the estimated parameters k_a and J, the values of q_{in}, q_T were calculated by Eq. 3 and 4 and are shown in Fig. 9. The decrease of the ingress rate, J from 4.1×10^{-9} to 1.6×10^{-9} mol/cm^2 s is mainly due to the reduction of the cathodic charge observed in the presence of underpotential deposited zinc (see Fig. 7) which causes a decrease of the charge density passed in q_{in} and of the charge density which is trapped (q_T). The anodic charge (q_a) is the difference between q_{in} and q_T and is given by[24]

$$q_a = FJ[t_c - (t_c/k_a)^{1/2}Q_T] \quad [7]$$

where Q_T is shown in Eq. 4 as a multiterm function of k_a and t_c. The monolayer coverage of zinc on the alloy blocks the adsorption of hydrogen atoms on the substrate.[28] Also, the hydrogen discharge on deposited zinc monolayer is negligible due to the low exchange current of this process on zinc.[29] Thus, the resultant cathodic current is reduced by the monolayer coverage of zinc which results in the decrease of ingress flux. Consequently, (as in Fig. 8), the observed decrease in q_a in the presence of a monolayer of Zn on the alloy surface can be attributed only to the observed decrease of the cathodic charge density observed in Fig. 7 and to the changes of the ingress flux. Note that k_a is constant and is independent of the processes which occur at the interface. Using the estimated parameters k_a and J, the theoretical charge passed was calculated in Eq. 2 and 5, and the results were compared with the experimental data in Fig. 10. Agreement has been obtained between the calculated and the experimental charge passed out values in the absence and presence of a monolayer deposited on the alloy surface.

Conclusion

The polarization experiments showed that underpotential deposition of zinc effectively inhibits the discharge of hydrogen up to 60% compared with the value obtained on the bare Monel K500. The Tafel slopes are in the range of 180 to 125 mV/decade which indicates that HER may be coupled discharge-recombination mechanism with the Langmuir isotherm of hydrogen surface coverage. By using a potentiostatic pulse technique, the trapping constant k_a was estimated to be 0.031 s^{-1}. A decrease of the ingress rate J from 4.1×10^{-9} to 1.6×10^{-9} mol/cm^2 s observed in the presence of underpotential-deposited zinc on the alloy and was mainly due to the reduction of the cathodic charge. The decrease in the ingress flux causes a decrease of the charge density passed and the charge density trapped in the alloy.

Acknowledgment

Technical assistance and financial support by A. John Sedriks, the Office of Naval Research, under Contract No. N00014-92-J-1434 are gratefully acknowledged.

Manuscript submitted Oct. 22, 1993; revised manuscript received Jan. 25, 1994.

The University of South Carolina assisted in meeting the publication costs of this article.

LIST OF SYMBOLS

c	surface hydrogen concentration, mol/cm^3
D_L	hydrogen diffusion coefficient, cm^2/s
D_a	apparent diffusion coefficient, cm^2/s
E	potential, V
E_{pdep}	predeposition potential, V
E_a	anodic potential, V
E_c	cathodic potential, V
E_{oc}	open-circuit potential, V
F	Faraday constant, 96,487 C/eq
i	current density, A/cm^2
J	ingress flux, mol/(cm^2 s)
k_a	$k\ D_a/D_L$ apparent trapping constant, s^{-1}
k	irreversible trapping constant, s^{-1}
K	equilibrium constant
q	charge density, C/cm^2
q_a	charge density passed out, C/cm^2
q_c	cathodic charge density, C/cm^2
q_{in}	charge density passed in, C/cm^2
q_T	charge density trapped, C/cm^2
Q_∞	dimensionless total charge passed
Q	$q/FJ\sqrt{t_c/k_a}$ dimensionless charge density
R	$k_a t_c$ dimensionless time
t	time, s
t_c	charge time, s

superscript ′ indicates the discharge process

REFERENCES

1. P. Subramanyan, in *Comprehensive Treatise of Electrochemistry,* Vol. 2, J. O'M. Bockris, B. E. Conway, E. Yeager, and R. E. White, Editors, p. 411, Plenum Press, New York (1981).
2. S. Bagaev and K. Pedan, *Zastita Metallov,* **19,** 968 (1983).
3. W. Beck, J. Jankowski, P. Fisher, S. Williams, and H. Bowen, *Report NADC-MA-7140,* p. 560, New York (1971).
4. J. P. Hirth, *Metall. Trans.*, **11A,** 861 (1980).
5. R. A. Oriani, *Rev. Mater. Sci.*, **8,** 327 (1978).
6. A. J. Kumnick and H. H. Johnson, *Metall. Trans.*, **6A,** 1087 (1975).
7. B. E. Wilde and T. Shimada, *Scripta Metall.*, **22,** 551 (1988).
8. P. J. Grobner, D. L. Sponseller, and D. E. Diesburg, *Corrosion,* **35,** 240 (1979).
9. M. Manohar, Ph.D. Thesis, The Ohio State University, Columbus, OH (1990).
10. B. E. Wilde and I. Chattoraj, *Scripta Metall.*, **26,** 627 (1992).
11. D. M. Drazic and L. Z. Vorkapic, *Corros. Sci.*, **18,** 907 (1978).
12. B. N. Popov, G. Zheng, and R. E. White, in *International Technical Conference Proceedings, SUR/FIN '93,* pp. 809-829, AESF, Orlando, FL (1993).
13. G. Zheng, B. N. Popov, and R. E. White, *This Journal,* **140,** 11, 3153 (1993).
14. G. Zheng, B. N. Popov, and R. E. White, in *International Technical Conference Proceedings, SUR/FIN '93,* pp. 779-791, AESF Orlando, FL (1993).
15. B. N. Popov, G. Zheng, and R. E. White, in *Corrosion Protection by Coatings and Surface Modification,* M. W. Kendig, K. Sugimoto, and N. R. Sorensen, Editors, PV 93-28, pp. 88-99, The Electrochemical Society Proceedings Series, Pennington, NJ (1993).
16. G. Zheng, B. N. Popov, and R. E. White, *ibid.*, pp. 100-111.
17. R. McKibben, R. M. Sharp, D. A. Harrington, B. G. Pound, and G. A. Wright, *Acta Metall.*, **35,** 253 (1987).
18. B. G. Pound, G. A. Wright, and R. M. Sharp, *ibid.*, **35,** 263 (1987).
19. F. Frumkin, in *Advances in Electrochemistry and Electrochemical Engineering,* Vol. 3, P. Delahay and C. W. Tobias, Editors, p. 163, Interscience, New York (1963).
20. J. McBreen and A. M. Genshow, in *Proceedings of Conference on Fundamental Aspects of Stress Corrosion Cracking,* p. 51, NACE, Houston, TX (1969).
21. R. M. Latanison and M. Kurkela, *Corrosion,* **39,** 174 (1983).
22. D. K. Kuhn and H. H. Johnson, *Acta Metall. Mater.*, **39,** 2901 (1991).
23. B. G. Pound, *Corrosion,* **45,** 18 (1989).
24. B. G. Pound, *Report SRI Project PYU-2969,* SRI, Thousand Oaks, CA (1992).
25. B. G. Pound, *J. Appl. Electrochem.*, **21,** 967 (1991).
26. B. G. Pound, *Corrosion,* **47,** 99 (1991).
27. B. G. Pound, *Acta Metall. Mater.*, **39,** 2099 (1991).
28. R. R. Adzic, in *Advances in Electrochemistry and Electrochemical Engineering,* Vol. 13, H. Gerisher and C. W. Tobias, Editors, p. 159, John Wiley & Sons, Inc., New York (1984).
29. S. Trasatti, *Z. Phys. Chem. N. F.,* **98,** 75 (1975).